# Crystal Structures of Human Carboxylesterase 1 in Covalent Complexes with the Chemical Warfare Agents Soman and Tabun[†,‡]

Christopher D. Fleming,[§] Carol C. Edwards,[||] Stephen D. Kirby,[⊥] Donald M. Maxwell,[⊥] Philip M. Potter,[||] Douglas M. Cerasoli,[⊥] and Matthew R. Redinbo*[,§]

*Department of Chemistry and Department of Biochemistry and Biophysics, University of North Carolina at Chapel Hill, Chapel Hill, North Carolina 27599, Department of Molecular Pharmacology, St. Jude Children's Research Hospital, Memphis, Tennessee 38105, and U.S. Army Medical Research Institute of Chemical Defense, Aberdeen Proving Ground, Maryland 21010*

*Received February 5, 2007; Revised Manuscript Received March 1, 2007*

ABSTRACT: The organophosphorus nerve agents sarin, soman, tabun, and VX exert their toxic effects by inhibiting the action of human acetylcholinesterase, a member of the serine hydrolase superfamily of enzymes. The current treatments for nerve agent exposure must be administered quickly to be effective, and they often do not eliminate long-term toxic side effects associated with organophosphate poisoning. Thus, there is significant need for effective prophylactic methods to protect at-risk personnel from nerve agent exposure, and protein-based approaches have emerged as promising candidates. We present the 2.7 Å resolution crystal structures of the serine hydrolase human carboxylesterase 1 (hCE1), a broad-spectrum drug metabolism enzyme, in covalent acyl-enzyme intermediate complexes with the chemical weapons soman and tabun. The structures reveal that hCE1 binds stereoselectively to these nerve agents; for example, hCE1 appears to react preferentially with the $10^4$-fold more lethal $P_S$ stereoisomer of soman relative to the $P_R$ form. In addition, structural features of the hCE1 active site indicate that the enzyme may be resistant to dead-end organophosphate aging reactions that permanently inactivate other serine hydrolases. Taken together, these data provide important structural details toward the goal of engineering hCE1 into an organophosphate hydrolase and protein-based therapeutic for nerve agent exposure.

The organophosphorus (OP[1]) nerve agents sarin, soman, tabun, and VX are among the deadliest synthetic chemicals (*1*). While the military use of OP nerve agents is widely banned, these compounds have been employed in recent decades by rogue states and terrorist groups. In 1988, Iraq employed weaponized sarin against its own Kurdish citizens in Halabja, a town adjacent to the Iranian border, killing an estimated 5000 (*2*). Coordinated attacks on the Tokyo subway system by the Japanese Aum Shinrikyo cult in 1995 also employed sarin, killing 12 and injuring nearly a thousand (*3*). The level of OP toxicity is striking, with $LD_{50}$ values for percutaneous exposure ranging from 1 g/person (tabun) to 10 mg/person (VX) (*1*). For these reasons, there is considerable interest in developing methods to detect OP nerve agents, to treat exposed patients, and to detoxify contaminated surfaces.

OP toxicity is thought to be mediated through the inhibition of human acetylcholinesterase (AcChE), a serine hydrolase responsible for processing the neurotransmitter acetylcholine and thus terminating cholinergic nerve impulses (*4*). The serine residue in the active site of AcChE is activated by adjacent histidine and glutamic acid residues, which together constitute the enzyme's catalytic triad (*5*). Nucleophilic attack on OPs by the active site serine displaces a strong leaving group from the chiral phosphate and creates a covalent acyl-enzyme intermediate (*6*). This reaction step has been reported to be $S_N2$, which would result in the stereoinversion of the chiral phosphate upon binding (*6*). Typically, acyl-enzyme intermediates in serine hydrolases are removed via hydrolysis, releasing an alcohol product; however, OPs have been observed to undergo an "aging" reaction that leads to a permanent alkyl−phosphate adduct bound to the catalytic serine. Aging, which involves dealkylation or, in the case of tabun, deamidation of the acyl-enzyme intermediate, has been hypothesized to proceed either through a hydrolytic (P−O or P−N bond scission) or a carbocation

[†] This work was supported, in part, by NIH Grants CA98468 and NS58089 and the American Lebanese Syrian Associated Charities.

[‡] Protein Data Bank codes are 2HRQ for the hCE1−soman structure and 2HRR for the hCE1−tabun structure.

* Corresponding author. Department of Chemistry, CB #3290, University of North Carolina at Chapel Hill, Chapel Hill, NC 27599-3290. Tel: (919) 843-8910. Fax: (919) 962-2388. E-mail: redinbo@unc.edu.

[§] University of North Carolina at Chapel Hill.

[||] St. Jude Children's Research Hospital.

[⊥] U.S. Army Medical Research Institute of Chemical Defense.

[1] Abbreviations: AcChE, human acetylcholinesterase; BuChE, human butyrylcholinesterase; CE, carboxylesterase; hCE1, human carboxylesterase 1; HI-6, 1-(2-hydroxy-iminomethylpyridinium)-1-(4-carboxyamino)-pyridinium dimethylether dichloride; *Mu*AcChE, *Mus musculus* acetylcholinesterase; OP, organophosphate; Ortho-7, 1,7-heptylene-bis-*N*,*N*′-2-pyridiniumaldoxime dichloride; PON1, human serum paraoxonase 1; rmsd, root mean square deviation; sarin, methylethyl methylphosphonofluoridate; soman, *O*-pinacolyl methylphosphonofluoridate; tabun, ethyl *N*,*N*-diemthylphosphoramidocyanidate; *Tc*AcChE, *Torpedo californica* acetylcholinesterase; VX, *O*-ethyl *S*-(2-diisopropylaminoethyl) methylphosphonothiolate; 2-PAM, pralidoxime chloride.

10.1021/bi700246n CCC: $37.00 © 2007 American Chemical Society
Published on Web 04/04/2007

(C−O bond scission) pathway (*7*). Prior to aging, the activity of the OP-inhibited serine hydrolases may be restored through reactivation of the catalytic serine with strong nucleophiles such as oximes; once aging occurs, however, reactivation is impossible with such methods (*1*). Aging of AcChE with nerve agents can occur within minutes (e.g., for soman) (*8*, *9*) or can take hours (e.g., for VX) (*7*).

The existing treatments for nerve agent exposure must be administered quickly to be effective, and they often do not eliminate long-term toxic side effects (*10*). Atropine, a muscarinic receptor antagonist, blocks cholinergic parasympathetic neurons to maintain capacity for respiration, and is typically administered as soon as possible after an OP exposure (*11*). Oxime reactivators like pralidoxime (2-PAM) or the Hagedom oxime HI-6 are also typically provided in an attempt to recover AcChE activity (*12*). Finally, an anticonvulsant like diazepam is commonly administered to treat seizures that can develop, albeit via unknown mechanisms (*13*). If this series of compounds is not given within minutes, however, victims quickly succumb (*10*). In addition, even if rapidly treated, many patients exposed to OP pesticides experience long-term brain damage, permanent electrocardiogram changes, or an "intermediate syndrome" associated with persistent muscle weakness (*14*).

There has been considerable interest in utilizing enzymes to detoxify OP nerve agents *in vivo*. Human butyrylcholinesterase (BuChE) shares 55% sequence identity and 0.8 Å root mean square deviation (rmsd) in Cα positions with human AcChE. While exhibiting no natural hydrolytic activity toward nerve agents (with $k_i$ values between 2.2 and $3.0 \times 10^5$ $M^{-1}$ $s^{-1}$ for sarin and VX, respectively), BuChE functions well as a bioscavenger, in that it binds and sequesters nerve agents as OP−enzyme complexes (*15*, *16*). Mutagenesis of residues adjacent to the BuChE active site led to the identification of variants that retain esterase activity and increase rates of reactivation 100-fold over the wild-type enzyme (*15*, *17*). Transgenic mice expressing one such mutant of human BuChE, Gly-117-His, have been shown to possess modestly increased resistance to intoxication by OP pesticides (*18*). In spite of these advances, an efficient prophylactic enzyme-based treatment for nerve agent exposure has remained elusive. Most mutant and wild-type forms of BuChE are subject to the same irreversible aging reactions as AcChE. Furthermore, relatively large doses of these stoichiometric scavenger enzymes must be administered for effective protection (*19*). For these reasons, additional enzymes have been examined for potential conversion into efficient OP hydrolases.

Human carboxylesterase 1 (hCE1) has been proposed as a candidate for development into an OP hydrolase (*20*−*22*). Carboxylesterases (CEs; EC 3.1.1.1) are members of the same serine hydrolase superfamily that contains AcChE and BuChE, and some CEs exhibit natural OP hydrolysis activity. For example, rat serum CE has been shown to metabolize sarin at least as efficiently as the Gly-117-His mutant form of human BuChE (*20*). hCE1 (78% identity to rat serum CE) metabolizes carboxylester, amine ester, and thioester linkages in a variety of endogenous and xenobiotic compounds (*22*−*24*). This glycoprotein shares 34% identity and 1.2 Å rmsd over Cα positions with AcChE, and utilizes the same two-step serine hydrolase catalytic mechanism. It has been shown that AcChE, BuChE, and mammalian CE exhibit a similar range of inhibition rate constants ($\log_{10} k_i$) of between 6.7 and 7.9 $M^{-1}$ $min^{-1}$ for soman (*21*). Several crystal structures of hCE1 have been determined, including complexes with heroin and cocaine analogues, the clinical therapeutics tamoxifen, tacrine, and mevastatin, and the endobiotics taurocholate, cholate, and coenzyme A (*25*−*28*). These structures highlight the promiscuous ability of the enzyme to bind a broad spectrum of structurally diverse compounds, a characteristic that would be important for an OP hydrolase with specificity for a variety of OP compounds. Here, we present the crystal structures of hCE1 in covalent acyl-enzyme intermediate complexes with the nerve agents soman and tabun. These structures reveal that hCE1 exhibits key structural differences in relation to the AcChE (*6*, *29*) and BuChE (*7*) complexes with OPs elucidated previously, features that may be exploited in the rational design of hCE1 into an efficient, broad-spectrum OP hydrolase.

## MATERIALS AND METHODS

*Nerve Agent Treatment and Crystallization.* A secreted form of hCE1 was expressed using baculovirus in *Spodoptera frugiperda* Sf21 cells and purified as previously described (*30*, *31*). Milligram quantities of purified enzyme were subsequently incubated with ∼10-fold molar excesses of racemic mixtures of soman (GD) and tabun (GA) (obtained from the Research Development and Engineering Command, Aberdeen Proving Ground, MD) for 1 h at room temperature. Excess agent was removed using size exclusion chromatography by passing the enzyme over PD-10 Sephadex G-25 columns (Amersham Biosciences, Uppsala, Sweden). The treated enzyme was tested to confirm the absence of both carboxylesterase activity (indicating complete inhibition of the hCE1) and the capacity to subsequently inhibit BuChE (indicating removal of unbound OP). Samples were then concentrated to 3−5 mg/mL using Amicon Ultra-15 (Millipore) spin concentrators. Long, platelike crystals (up to 500 $\mu$m × 100 $\mu$m × 40 $\mu$m) were grown by sitting drop vapor-diffusion methods in 9−13% PEG 3350, 0.1−0.4 M $Li_2SO_4$, 0.1 M citrate (pH 5.5), 0.1 M NaCl, 0.1 M LiCl, and 5% glycerol over a period of 1−4 weeks. Crystals were cryoprotected in stepwise fashion into 30% (w/v) sucrose plus mother liquor before cooling to 100 K in a liquid nitrogen cryostream.

*Structure Determination and Refinement*. Diffraction data were collected at 100 K at the Advanced Photon Source at Argonne National Laboratory (Argonne, IL) at beamline 22-ID (SER-CAT) for the hCE1−tabun complex, and at 23-IDD (GM/CA-CAT) for the hCE1−soman complex. Data were indexed and scaled using HKL-2000 (*32*). Molecular replacement was conducted using the program MolRep in the CCP4i suite (*33*) (v6.0) using one trimer of the hCE1−tacrine structure (RCSB PDB accession code 1MX1 (*26*)) as a search model. Refinement was accomplished using simulated annealing and torsion angle dynamics in CNS (*34*), and included an overall anisotropic *B*-factor and bulk solvent corrections as well as initial NCS restraints. A subset (7%) of the data for each structure were set aside for cross-validation by $R_{free}$ calculation prior to any structural refinement. Manual rebuilding was conducted using O (*35*) and $\sigma_a$-weighed electron density maps (*36*). Data collection and refinement statistics are outlined fully below (Table 1).

Table 1: Crystallographic Data Table

| | hCE1−soman | hCE1−tabun |
|---|---|---|
| resolution (Å)[a] | 50−2.70 (2.87−2.70) | 50−2.70 (2.80−2.70) |
| space group | $P2_1$ | $P2_12_12_1$ |
| asymmetric unit | two trimers | one trimer |
| cell constants (Å, deg) | $a = 55.5$ | $a = 55.6$ |
| | $b = 181.2$ | $b = 181.1$ |
| | $c = 203.1$ | $c = 202.9$ |
| | $\alpha = \gamma = 90$ | $\alpha = \beta = \gamma = 90$ |
| | $\beta = 89.9$ | |
| total reflections | 108 029 | 53 127 |
| unique reflections | 29 197 | 8301 |
| mean redundancy[a] | 3.7 (3.3) | 6.4 (6.3) |
| $R_{sym}$ (%)[a,b] | 10.2 (21.6) | 11.7 (29.2) |
| Wilson $B$ factor (Å$^2$) | 34.6 | 28.8 |
| completeness (%)[a] | 99.9 (99.9) | 91.8 (93.8) |
| mean $I/\sigma$[a] | 19.7 (7.8) | 21.8 (7.7) |
| $R_{cryst}$ (%)[a,c] | 17.0 | 16.7 |
| $R_{free}$ (%)[a,d] | 22.5 | 23.2 |
| RCSB access codes | 2HRQ | 2HRR |

[a] Number in parentheses is for the highest shell. [b] $R_{sym} = \sum|I - \langle I\rangle|/\sum I$, where $I$ is the observed intensity and $\langle I\rangle$ is the average intensity of multiple symmetry-related observations of that reflection. [c] $R_{cryst} = \sum||F_o| - |F_c||/\sum|F_o|$, where $F_o$ and $F_c$ are the observed and calculated structure factors, respectively. [d] $R_{free} = \sum||F_o| - |F_c||/\sum|F_o|$ for 7% of the data not used at any stage of structural refinement.

Final structures were validated using PROCHECK (*37*), and all figures were generated in PyMol (http://pymol.sourceforge.org (*38*)).

## RESULTS

*Crystallographic Analysis.* The hCE1−soman and hCE1−tabun complex structures were determined by molecular replacement, and refined to 2.7 Å resolution in space group $P2_1$ (hCE1−soman) or $P2_12_12_1$ (hCE1−tabun). These space groups have been observed in previous hCE1 structures (*25*−*28*), and correspond to either two ($P2_1$, hCE1−soman) or one ($P2_12_12_1$, hCE1−tabun) trimer per asymmetric unit. While the cell constants of the hCE1−soman structure appear to be capable of adapting $P2_12_12_1$ space group symmetry, $R_{sym}$ values establish $P2_1$ as correct for this complex. The initial maps were of high quality, and were easily traceable for any deviations that occurred between the search model and the new structures. The final $R$ factors were 17.0% ($R_{cryst}$) and 22.5% ($R_{free}$) for the hCE1−soman complex and 16.7% ($R_{cryst}$) and 23.0% ($R_{free}$) for the hCE1−tabun complex (Table 1).

*Domain Architecture of hCE1.* The 62 kDa hCE1 monomer is composed of three domains and two ligand binding sites (Figure 1). The catalytic domain exhibits the canonical $\alpha/\beta$-hydrolase fold and contains a high-mannose glycosylation site at Asn79 that is critical to protein stability and function (*27*). The $\alpha\beta$ and regulatory domains sit adjacent to the active site, with the latter flanking the surface ligand-binding site termed the Z-site (*27*). The binding of various small molecules to the Z-site has been shown to regulate a trimer−hexamer equilibrium of hCE1. In both structures presented here, the Z-site contains bound sucrose, the crystallographic cryoprotectant utilized in these studies (Figure 1). The active site of the enzyme is located at the interface of the three domains and is composed of the catalytic triad Ser221, His468, and Glu354. The hCE1 trimer exhibits $C3$ symmetry and is formed largely by contacts

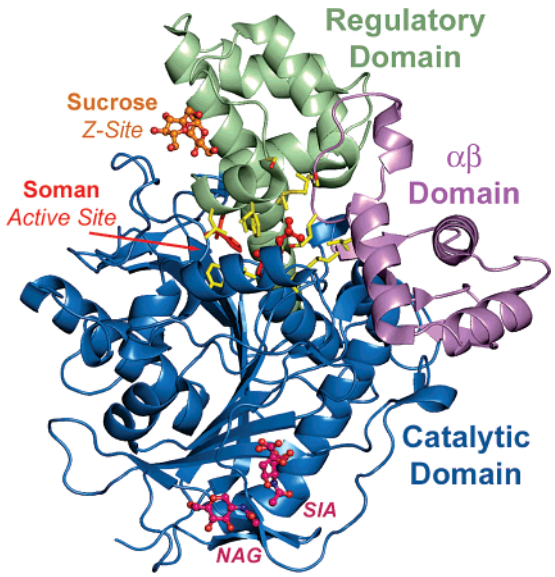


FIGURE 1: The overall monomeric structure of hCE1 bound to soman. The catalytic domain is shown in blue, the regulatory domain in green, and the $\alpha\beta$ domain in purple. Active site residues are highlighted in yellow, with the catalytic triad and soman adduct in red. The Z-site is occupied by sucrose, modeled as ball-and-stick in orange. The carbohydrates attached to residue Asn79 are shown ball-and-stick in magenta, of which only the initial *N*-acetylglucosamine (NAG) and terminal sialic acid (SIA) are observed.

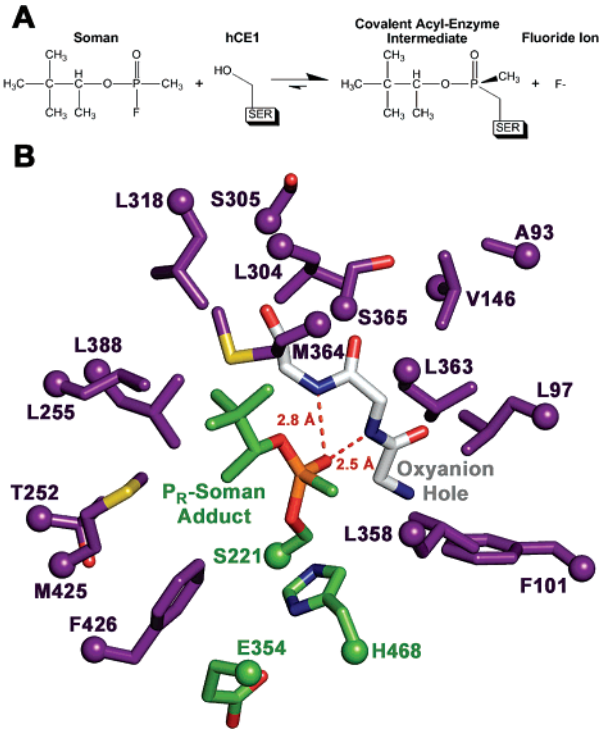


FIGURE 2: hCE1−soman complex. (A) Chemical scheme of soman reacting with hCE1. Soman is attacked at the chiral phosphate by the O$\gamma$ of Ser221, resulting in a covalent acyl-enzyme intermediate and a free fluoride ion. (B) Cutaway view of the active site of hCE1 bound covalently to soman. Surrounding residues are shown in purple, the catalytic triad and soman adduct in green, and the oxyanion hole in white. Hydrogen bonds between the phosphoryl oxygen and the oxyanion hole are shown in red.

between the $\alpha\beta$ domains of each monomer (not shown) (*25*, *27*, *28*). A hexamer has also been observed for hCE1 in which two trimers are stacked with their active sites facing

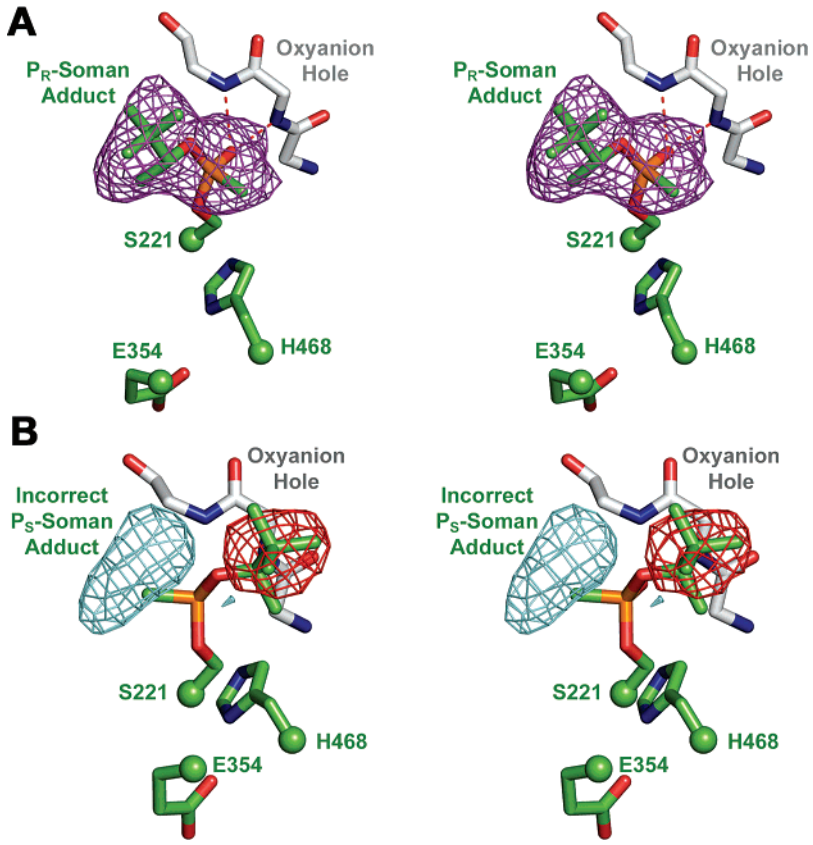


FIGURE 3: Stereochemistry of the hCE1−soman adduct. The catalytic triad of amino acids (Ser221, His468, and Glu 354) and the adduct are shown in green, with the oxyanion hole in white. (A) Stereoview of a 2.7 Å resolution $F_o - F_c$ simulated annealing omit map (purple, contoured to 3$\sigma$) calculated for the $P_R$−soman adduct. (B) Stereoview of initial difference density maps for the incorrect $P_S$−soman adduct (cyan for positive, shown at 3$\sigma$; red for negative, shown at −3$\sigma$).

in and with the Z-site loops interdigitating (*26*, *27*); neither of the structures described here forms a hexamer, however.

*Structure of the hCE1−Soman Complex.* Initial difference density ($F_o - F_c$) maps in the hCE1−soman structure indicated a 7$\sigma$ electron density peak 1.6 Å away from the O$\gamma$ of Ser221 in all six active site cavities, suggesting the presence of a covalently attached phosphoryl adduct. At lower $\sigma$ levels (e.g., 3−5$\sigma$), the maps revealed additional density to suggest the presence of the acyl-enzyme intermediate, in which the fluoride ion has been displaced by the attack of the enzyme's catalytic serine (Figure 2A). This intermediate was built into the model using this electron density and refined well, yielding a covalent adduct at the active site that exhibits $P_R$ stereochemistry for the chiral phosphorus atom (Figure 2B). The covalent adduct is stabilized by two hydrogen bonds (2.8 Å and 2.5 Å) between the phosphoryl oxygen and the main-chain nitrogens of Gly141 and Gly143 in the enzyme's oxyanion hole. The large, methylpinacolyl alkoxy group of the soman adduct is directed toward the spacious region of the active site cavity adjacent to Met364, while the methyl group occupies the smaller, rigid pocket near Phe101. This rigid pocket has been previously shown to select for the small acetyl and methyl ester linkages in heroin and cocaine (*27*).

The $P_R$ stereochemistry observed for the covalent adduct in this structure suggests that hCE1 selectively reacted with the $P_S$ stereoisomer of soman, which is 10000-fold more effective than $P_R$ at inhibiting AcChE (*39*), based on an $S_N2$ stereoinversion (*40*, *41*). A 2.7 Å resolution simulated annealing omit map confirmed the stereochemistry of the covalent adduct (Figure 3A). We also placed the presumably incorrect $P_S$ stereoisomer into the original model (before refinement or any ligands were added) and performed one round of structural refinement. Distinct positive and negative difference density ($|F_{obs} - F_{calc}|$, $\phi_{calc}$) peaks support the conclusion that the acyl-enzyme intermediate observed in the structure is in the *R* conformation (Figure 3B). Structural constraints in the hCE1 active site also indicate that $P_S$−soman is unlikely to be processed by the enzyme because this stereoisomer's alkoxy group is too large to be accommodated in the small, rigid pocket of the catalytic gorge. Soman also contains a second stereocenter located at the C5 atom in the methylpinacolyl alkoxy group. While it is observed in the $C_R$ orientation in this structure, there appear to be no structural constraints that would prevent the $C_S$ orientation from being accommodated in the hCE1 active site. Taken together, these data suggest that hCE1 is selective for the lethal $P_S$ stereoisomer of soman.

*Structure of the hCE1−Tabun Complex.* Similar to the hCE1−soman structure, initial difference density in the hCE1−tabun structure indicated that the active site Ser221 in this structure had been covalently modified. Subsequent refinement confirmed the presence in the hCE1 active site of the acyl-enzyme intermediate of tabun, which is generated by the replacement of the cyano group with the enzyme's catalytic serine (Figure 4A, B). In this covalent complex, the alkoxy group is positioned in the large pocket adjacent to Met364, while the *N*,*N*-dimethylamine group is located in the smaller, rigid pocket; these are orientations similar to those observed in the hCE1−soman complex. The covalent

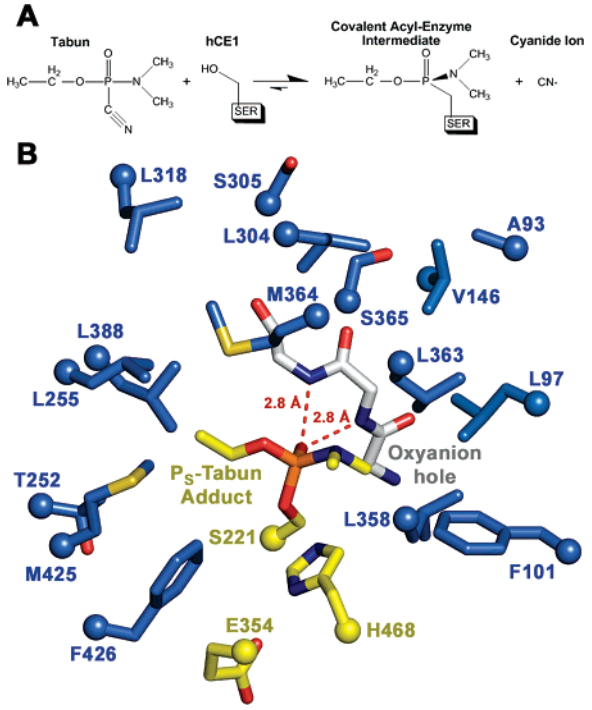


FIGURE 4: hCE1−tabun complex. (A) Chemical scheme of tabun reacting with hCE1. Tabun is attacked at the chiral phosphate by the O$\gamma$ of Ser221, resulting in a covalent acyl-enzyme intermediate and free cyanide ion. (B) Cutaway view of the hCE1 active site covalently bound to tabun. Surrounding residues are shown in blue, the catalytic triad and adduct in yellow, and the oxyanion hole in white. Hydrogen bonds between the adduct and the oxyanion hole (dashed lines) are shown in red.

adduct in this structure exhibits $P_S$ stereochemistry, which indicates that the protein molecules in the crystal reacted with the $P_R$ isoform of tabun. As with soman, simulated annealing omit map was used to confirm the stereochemistry of the adduct (Figure 5A). This revealed that the correct adduct stereoisomer was placed in the active site cavity. We also placed the presumably incorrect $P_R$ stereoisomer into the original model (prior to any refinement or the addition of ligands) and conducted one round of structural refinement. While the resultant difference density maps were not as dramatic as those obtained for the incorrect $P_S$ adduct of soman (due to the similarity in size between the two R groups of tabun), they support the conclusion that the stereochemistry of the hCE1−tabun adduct is $P_S$, and indicate that the hCE1 molecules present in the crystal examined reacted with $P_R$−tabun (Figure 5B).

*Comparison to Cholinesterase−Nerve Agent Structures.* We next compared the hCE1 complexes reported here to two covalent acyl-enzyme intermediate complexes of AcChE with nerve agents: the *Mus musculus (Mu)* AcChE with tabun (*42*) and the *Torpedo californica (Tc)* AcChE with VX (*29*). The *Mu*AcChE−tabun complex exhibits an acyl-enzyme intermediate in the $P_R$ conformation, indicating that the enzyme reacted with the $P_S$ form of tabun (Figure 6A). This observation is in agreement with the work of Degenhart et al. that shows AcChE is inhibited 6-fold more readily by $P_S$−tabun relative to the $P_R$ isoform (*43*). Note, however, that hCE1 and AcChE exhibit acyl-enzyme intermediates with the opposite stereochemistry: $P_S$ for hCE1 and $P_R$ for AcChE (Figure 6A). The structure of *Tc*AcChE in covalent complex with VX reveals a $P_R$ covalent adduct, indicating that the enzyme reacted with the *S*-isomer of VX ($VX_S$) (Figure 6B). $VX_S$ is known to be 115-fold more potent than $VX_R$ toward AcChE (*44*). Relative to hCE1, the *Tc*AcChE−VX complex also exhibits alternative organization of its active site with respect to the acyl-enzyme intermediate. The *Tc*AcChE−VX complex places its larger ethoxy group adjacent to H400, while hCE1 positions the larger methylpinacolyl alkoxy group of its soman complex away from its catalytic H468 (Figure 6B). Although limited biochemical work has been conducted with CEs and their stereoselectivity toward nerve agents, the guinea pig serum CE is known to be 100-fold more susceptible to $P_S$−soman (*45*), in accordance with the structural data presented above for hCE1. Taken together, these observations support the conclusion that the hCE1 acyl-enzyme intermediates observed are formed via an $S_N2$-like stereoinversion, and generate distinct covalent complexes relative to the cholinesterases.

The two covalent hCE1 complexes presented here also indicate that hCE1 does not undergo aging (dealkylation) when inhibited by soman or tabun. While the volumes of the catalytic gorges of hCE1, AcChE, and BuChE are similar (924, 993, 982 Å$^3$, respectively) (*46*), their active site architectures are significantly distinct. These differences are largely generated by the position of the so-called "acyl" loop, which has been previously suggested to be involved in the aging process of AcChE (*6*). The acyl loops of the cholinesterases place large phenylalanine or leucine residues adjacent to the catalytic serine, producing a small pocket that can accommodate the acyl group of an OP but not the larger alkoxy groups of nerve agents like soman (Figure 7). As a consequence, the alkoxy moieties in these cholinesterase structures are within ~3.5 Å of the catalytic triad His (Figure 6), which has been proposed to facilitate aging (*6*, *29*, *42*). In contrast, in hCE1 the corresponding loop is shifted by ~7 Å away from the adduct and is stabilized by two rigid proline residues, which generate the large pocket that accommodates the alkoxy group in the soman- and tabun-bound structures presented here (Figures 2, 4, 6). These binding modes position the alkoxy oxygens outside hydrogen-bonding range (4.7−5.1 Å) with respect to His468 of the hCE1 catalytic triad. Note that while this histidine is static in position in the hCE1 structures determined to date, it has been observed to shift in other cholinesterase structures (*29*, *42*). If one imposes this shift on the hCE1 histidine, however, it would only come within 4.4 Å of the alkoxy oxygen of the hCE1 acyl-enzyme intermediates. Thus, the distinct architecture of the hCE1 active site appears unfavorable to the process of aging because the alkoxy group moiety is placed relatively distant from the catalytic histidine. Indeed, the >1 week time frame necessary for the hCE1−nerve agent crystals to grow would presumably provide sufficient time for aging to occur. The fact that a secondary dealkylation reaction is not observed in the structures presented here supports the conclusion that hCE1 may be resistant to this process. However, it remains possible (though unlikely) that the crystallization process may have selected only for nonaged hCE1 complexes. As discussed below, lack of aging could not be confirmed by the standard experimental method of reactivation using an oxime.

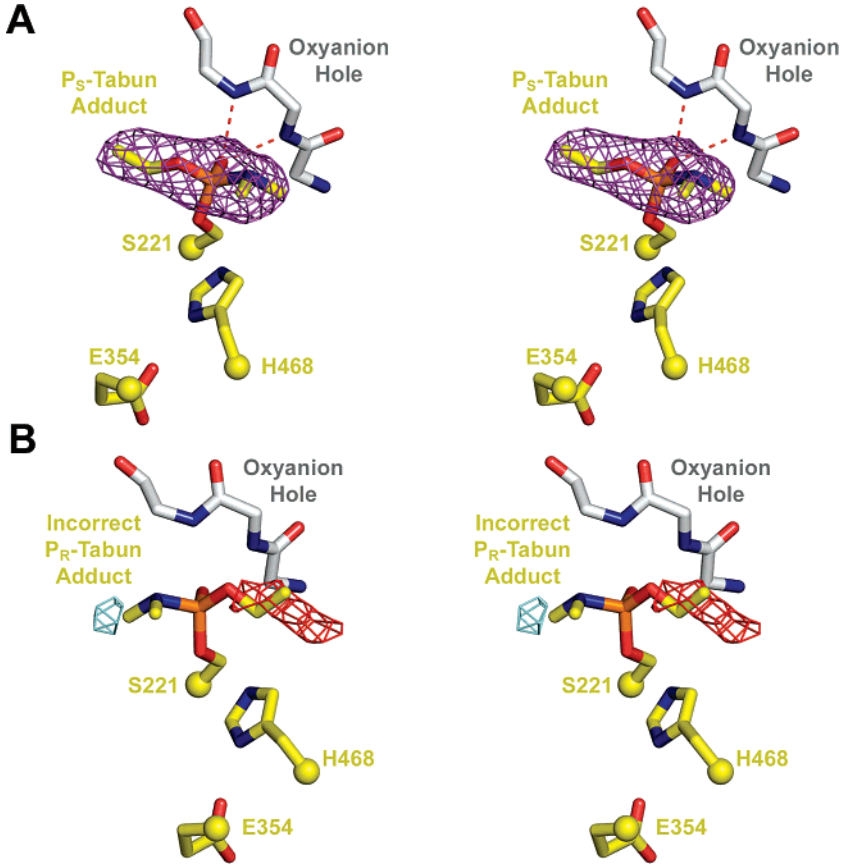


FIGURE 5: Stereochemistry of the hCE1−tabun adduct. The catalytic triad and adduct are shown in yellow, with the oxyanion hole in white. (A) Stereoview of a 2.7 Å resolution $F_o - F_c$ simulated annealing omit map (purple, contoured to 3$\sigma$) calculated for the $P_S$−tabun adduct. (B) Stereoview of initial difference density maps for the incorrect $P_R$−tabun adduct (cyan for positive, shown at 2$\sigma$; red for negative, shown at −2$\sigma$).

## DISCUSSION

The hCE1−nerve agent complex structures presented here are of covalent acyl-enzyme intermediates rather than the fully aged products. This result was unexpected because the trapping of the cholinesterases (AcChE, BuChE) in nonaged, acyl-enzyme intermediate complexes required the exposure of pregrown crystals to nerve agents immediately prior to X-ray data collection (*7*, *29*, *42*). In contrast, the hCE1−nerve agent complex crystals used to produce the structures reported here were generated after the enzyme was exposed to nerve agents in solution, and then crystallized over 1−4 weeks. This time frame would be expected to allow for sufficient time for aging to occur (*7*).

Aging is defined experimentally by the inability of the OP-treated enzyme to be reactivated by a strong nucleophile like an oxime, which are able to displace a covalent acyl-enzyme intermediate but not a covalent aged complex (*1*, *11*). We examined the ability of the oximes diacetylmonoxime and monoisonitrosoacetone, which are effective with both cholinesterases and rat serum carboxylesterase (*21*), to reactivate tabun- and soman-inhibited hCE1. However, no enzyme reactivation was detected (data not shown), perhaps because hCE1, like other intracellular liver CEs from guinea pig (*47*) and rat (D. Maxwell, unpublished data), is not reactivated by these oximes. Indeed, analysis of the active site of *Mu*AcChE bound to the oximes HI-6, Ortho-7, and obidoxime reveals that a series of aromatic residues are required for stabilization and proper alignment of the oxime nucleophiles for reactivation (*48*); these aromatic residues are not present in the active site of hCE1. In the absence of oxime reactivation of the inhibited hCE1, it is impossible to experimentally confirm a lack of aging after inhibition by soman or tabun. Additional work to identify an oxime that can reactivate hCE1 might allow this protein to function as a "pseudocatalytic" scavenger (*49*).

Several structural features of the hCE1−nerve agent complexes presented here indicate that hCE1 may be resistant to aging. Detailed structural studies of nerve agent−cholinesterase complexes reported previously have highlighted the importance of the catalytic histidine in aging, either via hydrolysis or via carbocation stabilization (*6*, *29*, *42*). As shown above, the active site of hCE1 is distinct from the cholinesterases in terms of interactions with nerve agents (Figures 6 and 7). In hCE1, the alkoxyl substituent is positioned away from the catalytic histidine in the active site gorge, while the chlolinesterases place this group in close proximity to their catalytic histidines. Controversy still exists over the mechanism of aging for some nerve agents. For example, mass spectrometry and X-ray crystallographic studies of the AcChE−tabun complex indicate that aging occurs via the loss of the dimethylamine group through P−N bond scission rather than by loss of the alkoxy group (*42*, *50*). The mechanism proposed involves the protonation of the dimethylamine nitrogen by the catalytic histidine (*42*). Both aged and nonaged *Mu*AcChE−tabun complex structures appear to contradict this mechanism, however, because the

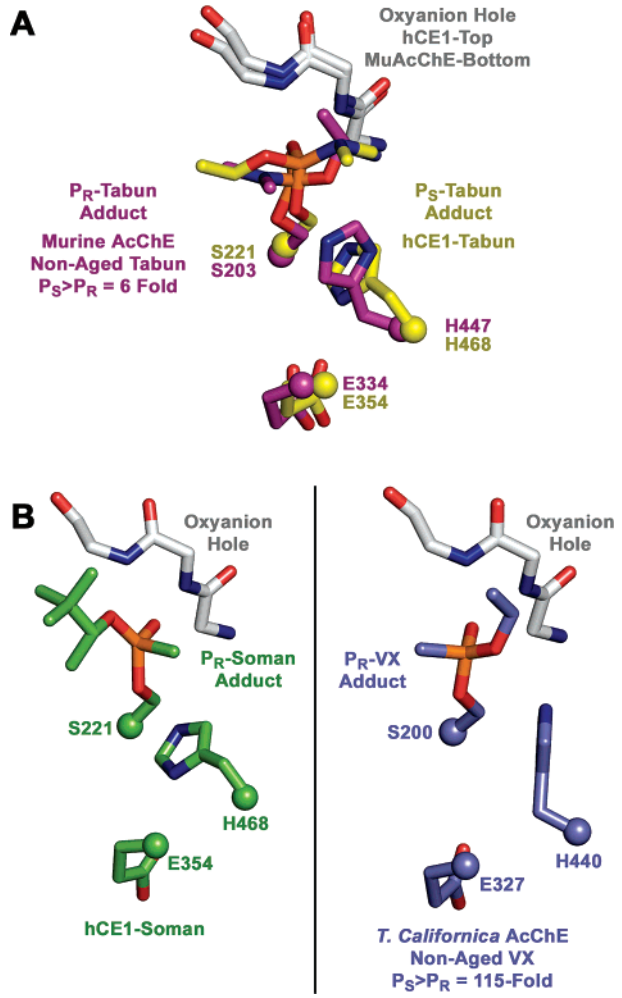


FIGURE 6: Comparison between hCE1−nerve agent complexes and nonaged nerve agent−cholinesterase complexes (the oxyanion hole in each structure is rendered in white). (A) Superposition of hCE1−tabun complex (yellow) with the nonaged complex of murine AcChE (*42*) structure with tabun (purple). (B) The hCE1−soman complex (green) is on the left, with the nonaged *Tc*AcChE−VX complex (*29*) on the right (blue).

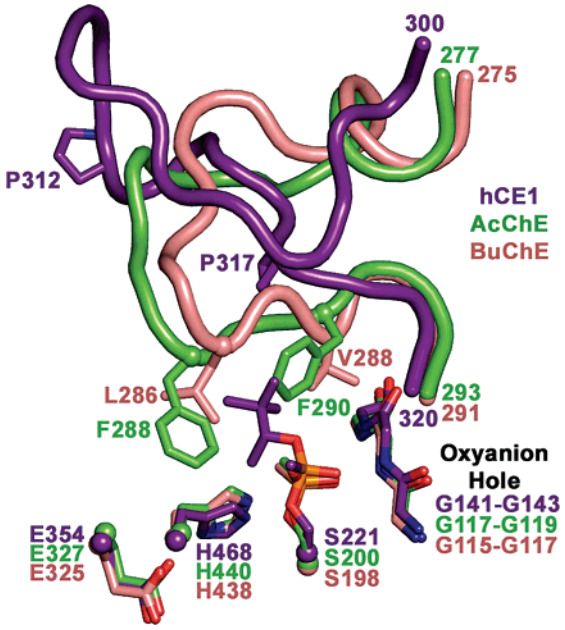


FIGURE 7: The acyl-loop regions of the aged AcChE−soman (*6*) complex (green) and the aged BuChE−echothiophate (*7*) complex (salmon) superimposed on that of the nonaged hCE1−soman complex (purple).

dimethylamine group is pointing away from the catalytic histidine (*42*) (Figure 6A). In addition, we found no evidence for aging of the hCE1−tabun structure (Figure 5), even though the dimethylamine group is proximal to His468. Regardless however, new methods must be developed to experimentally examine the ability of hCE1 to age in the presence of organophosphorus nerve agents.

Inspired by the identification of cholinesterase mutants with favorable features in relation to organophosphate binding and hydrolysis (*15*, *17*, *51*, *52*), the structures of hCE1 in complexes with nerve agents presented here may be useful in developing this enzyme into a protective nerve agent hydrolase. Use of enzymes as a prophylaxis for OP exposure carries significant benefits beyond current chemical treatments. A prophylactic treatment for nerve agent exposure would be designed to protect at-risk military personnel and civilian first responders. As such, the use of a human enzyme for such a purpose would be expected to avoid potentially harmful immune responses that may arise from protein-based therapies derived from nonhuman sources. Extensive work has been conducted toward this goal with a recombinant form of BuChE purified from the milk of transgenic goats (*49*, *53*). While this enzyme has been shown to confer a level of protection up to 5.5 × $LD_{50}$ for VX and soman in guinea pigs (*49*), it acts purely as a stoichiometric bioscavenger and binds to, but does not catalytically inactivate, nerve agents. Thus, protection levels are limited stoichiometrically to the dose given. The most promising catalytic bioscavenger identified to date is the organophosphorus hydrolase (also known as phosphotriesterase) from the bacterium *Pseudomonas diminuta*; this enzyme exhibits moderate activity ($k_{cat}$ = 56 $s^{-1}$ for sarin, 77 $s^{-1}$ for tabun) for breaking down nerve agents (*54*, *55*). However, the bacterial origin of this organophosphorus hydrolase may limit its effectiveness in humans (*49*). The human serum enzyme paraoxonase 1 (PON1) has been examined for development, but no structural data and low catalytic efficiency for nerve agents have plagued this process (*49*). Therefore, a human enzyme with catalytic ability to hydrolyze nerve agents efficiently would be a welcome addition to this growing field of protein-based potential therapeutics.

Several features of hCE1 make it a promising candidate for development into a catalytic prophylactic for nerve agent exposure. As a human enzyme, it is unlikely to elicit an immune response; indeed, cross-species injections of CEs have established that these enzymes can circulate stably within mammalian serum for weeks (*20*, *21*). hCE1 is also a naturally broad-spectrum enzyme that acts on a wide range of structurally distinct substrates; thus, protection against several nerve agents may be possible. Finally, as described above, the active site of hCE1 may be uniquely resistant to the secondary dealkylation reaction that can result in aging after inhibition by an OP nerve agent. Taken together, these observations suggest that if hCE1 were converted into an efficient OP hydrolase, it may be an effective protein-based therapeutic that detoxifies organophosphate chemical weapons.

## ACKNOWLEDGMENT

The authors thank J. Orans, D. Teotico, M. Miley, and E. Ortlund for experimental assistance and pertinent discussions. We also thank the support staff at SER-CAT and GM/CA-CAT at APS for assistance with data collection. Use of the Advanced Photon Source was supported by the U.S. Department of Energy, Office of Science, Office of Basic Energy Sciences, under Contract No. W-31-109-Eng-38.

## REFERENCES

1. Wiener, S. W., and Hoffman, R. S. (2004) Nerve agents: a comprehensive review, *J. Intensive Care Med. 19*, 22−37.
2. Newmark, J. (2004) The birth of nerve agent warfare: lessons from Syed Abbas Foroutan, *Neurology 62*, 1590−1596.
3. Lee, E. C. (2003) Clinical manifestations of sarin nerve gas exposure, JAMA *290*, 659−662.
4. Casida, J. E., and Quistad, G. B. (2004) Organophosphate toxicology: safety aspects of nonacetylcholinesterase secondary targets, *Chem. Res. Toxicol. 17*, 983−998.
5. Kraut, J. (1977) Serine proteases: structure and mechanism of catalysis, *Annu. Rev. Biochem. 46*, 331−358.
6. Millard, C. B., Kryger, G., Ordentlich, A., Greenblatt, H. M., Harel, M., Raves, M. L., Segall, Y., Barak, D., Shafferman, A., Silman, I., and Sussman, J. L. (1999) Crystal structures of aged phosphonylated acetylcholinesterase: nerve agent reaction products at the atomic level, *Biochemistry 38*, 7032−7039.
7. Nachon, F., Asojo, O. A., Borgstahl, G. E., Masson, P., and Lockridge, O. (2005) Role of water in aging of human butyrylcholinesterase inhibited by echothiophate: the crystal structure suggests two alternative mechanisms of aging, *Biochemistry 44*, 1154−1162.
8. Saxena, A., Viragh, C., Frazier, D. S., Kovach, I. M., Maxwell, D. M., Lockridge, O., and Doctor, B. P. (1998) The pH dependence of dealkylation in soman-inhibited cholinesterases and their mutants: further evidence for a push-pull mechanism, *Biochemistry 37*, 15086−15096.
9. Shafferman, A., Ordentlich, A., Barak, D., Stein, D., Ariel, N., and Velan, B. (1996) Aging of phosphylated human acetylcholinesterase: catalytic processes mediated by aromatic and polar residues of the active centre, *Biochem. J. 318* (Part 3), 833−840.
10. Newmark, J. (2004) Therapy for nerve agent poisoning, *Arch. Neurol. 61*, 649−652.
11. Bajgar, J. (2004) Organophosphates/nerve agent poisoning: mechanism of action, diagnosis, prophylaxis, and treatment, *Adv. Clin. Chem. 38*, 151−216.
12. Eyer, P. (2003) The role of oximes in the management of organophosphorus pesticide poisoning, *Toxicol. Rev. 22*, 165−190.
13. Marrs, T. C. (2004) The role of diazepam in the treatment of nerve agent poisoning in a civilian population, *Toxicol. Rev. 23*, 145−157.
14. Brown, M. A., and Brix, K. A. (1998) Review of health consequences from high-, intermediate- and low-level exposure to organophosphorus nerve agents, *J. Appl. Toxicol. 18*, 393−408.
15. Millard, C. B., Lockridge, O., and Broomfield, C. A. (1995) Design and expression of organophosphorus acid anhydride hydrolase activity in human butyrylcholinesterase, *Biochemistry 34*, 15925−15933.
16. Raveh, L., Grunwald, J., Marcus, D., Papier, Y., Cohen, E., and Ashani, Y. (1993) Human butyrylcholinesterase as a general prophylactic antidote for nerve agent toxicity. In vitro and in vivo quantitative characterization, *Biochem. Pharmacol. 45*, 2465−2474.
17. Millard, C. B., Lockridge, O., and Broomfield, C. A. (1998) Organophosphorus acid anhydride hydrolase activity in human butyrylcholinesterase: synergy results in a somanase, *Biochemistry 37*, 237−247.
18. Wang, Y., Boeck, A. T., Duysen, E. G., Van Keuren, M., Saunders, T. L., and Lockridge, O. (2004) Resistance to organophosphorus agent toxicity in transgenic mice expressing the G117H mutant of human butyrylcholinesterase, *Toxicol. Appl. Pharmacol. 196*, 356−366.
19. Raveh, L., Grauer, E., Grunwald, J., Cohen, E., and Ashani, Y. (1997) The stoichiometry of protection against soman and VX toxicity in monkeys pretreated with human butyrylcholinesterase, *Toxicol. Appl. Pharmacol. 145*, 43−53.
20. Maxwell, D. M., and Brecht, K. M. (2001) Carboxylesterase: specificity and spontaneous reactivation of an endogenous scavenger for organophosphorus compounds, *J. Appl. Toxicol. 21* (Suppl. 1), S103−S107.
21. Maxwell, D. M., Brecht, K. M., Saxena, A., Feaster, S., and Doctor, B. P. (1998) Comparison of Cholinesterases and Carboxylesterase as Bioscavengers for Organophosphorus Compounds, in *Structure and Function of Cholinesterases and Related Proteins* (Doctor, B. P., Ed.) pp 387−392, Plenum Press, New York.
22. Redinbo, M. R., and Potter, P. M. (2005) Mammalian carboxylesterases: from drug targets to protein therapeutics, *Drug Discovery Today 10*, 313−325.
23. Satoh, T., and Hosokawa, M. (1998) The mammalian carboxylesterases: from molecules to functions, *Annu. Rev. Pharmacol. Toxicol. 38*, 257−288.
24. Satoh, T., and Hosokawa, M. (2006) Structure, function and regulation of carboxylesterases, *Chem. Biol. Interact. 162*, 195−211.
25. Bencharit, S., Edwards, C. C., Morton, C. L., Howard-Williams, E. L., Kuhn, P., Potter, P. M., and Redinbo, M. R. (2006) Multisite promiscuity in the processing of endogenous substrates by human carboxylesterase 1, *J. Mol. Biol. 363*, 201−214.
26. Bencharit, S., Morton, C. L., Hyatt, J. L., Kuhn, P., Danks, M. K., Potter, P. M., and Redinbo, M. R. (2003) Crystal structure of human carboxylesterase 1 complexed with the Alzheimer's drug tacrine: from binding promiscuity to selective inhibition, *Chem. Biol. 10*, 341−349.
27. Bencharit, S., Morton, C. L., Xue, Y., Potter, P. M., and Redinbo, M. R. (2003) Structural basis of heroin and cocaine metabolism by a promiscuous human drug-processing enzyme, *Nat. Struct. Biol. 10*, 349−356.
28. Fleming, C. D., Bencharit, S., Edwards, C. C., Hyatt, J. L., Tsurkan, L., Bai, F., Fraga, C., Morton, C. L., Howard-Williams, E. L., Potter, P. M., and Redinbo, M. R. (2005) Structural insights into drug processing by human carboxylesterase 1: tamoxifen, mevastatin, and inhibition by benzyl, *J. Mol. Biol. 352*, 165−177.
29. Millard, C. B., Koellner, G., Ordentlich, A., Shafferman, A., Silman, I., and Sussman, J. (1999) Reaction products of acetylcholinesterase and VX reveal a mobile histidine in the catalytic triad, *J. Am. Chem. Soc. 121*, 9883−9884.
30. Danks, M. K., Morton, C. L., Krull, E. J., Cheshire, P. J., Richmond, L. B., Naeve, C. W., Pawlik, C. A., Houghton, P. J., and Potter, P. M. (1999) Comparison of activation of CPT-11 by rabbit and human carboxylesterases for use in enzyme/prodrug therapy, *Clin. Cancer Res. 5*, 917−924.
31. Morton, C. L., and Potter, P. M. (2000) Comparison of Escherichia coli, Saccharomyces cerevisiae, Pichia pastoris, Spodoptera frugiperda, and COS7 cells for recombinant gene expression. Application to a rabbit liver carboxylesterase, *Mol. Biotechnol. 16*, 193−202.
32. Otwinowski, Z., and Minor, W. (1997) Processing of X-ray Diffraction Data Collected in Oscillation Mode, in *Macromolecular Crystallography, part A* (Carter, C., Jr., and Sweet, R., Eds.) pp 307−326, Academic Press, New York.
33. (1994) The CCP4 suite: programs for protein crystallography, *Acta Crystallogr. D Biol. Crystallogr. 50*, 760−763.
34. Brunger, A. T., Adams, P. D., Clore, G. M., DeLano, W. L., Gros, P., Grosse-Kunstleve, R. W., Jiang, J. S., Kuszewski, J., Nilges, M., Pannu, N. S., Read, R. J., Rice, L. M., Simonson, T., and Warren, G. L. (1998) Crystallography & NMR system: A new software suite for macromolecular structure determination, *Acta Crystallogr. D Biol. Crystallogr. 54*, 905−921.
35. Jones, T. A., Zou, J. Y., Cowan, S. W., and Kjeldgaard, M. (1991) Improved methods for building protein models in electron density maps and the location of errors in these models, *Acta Crystallogr. A 47* (Part 2), 110−119.
36. Read, R. J. (1986) Improved Fourier Coefficients for maps using phases from partial structures with errors, *Acta Crysallogr. A 42*, 140−149.
37. Laskowski, R. A., MacArthur, M. W., Moss, D. S., and Thornton, J. M. (1993) PROCHECK: a program to check the stereochemical quality of protein structures, *J. Appl. Crystallogr. 26*, 283−291.
38. DeLano, W. L. (2002) DeLano Scientific, Palo Alto, CA.
39. Benschop, H. P., Konings, C. A., Van Genderen, J., and De Jong, L. P. (1984) Isolation, anticholinesterase properties, and acute toxicity in mice of the four stereoisomers of the nerve agent soman, *Toxicol. Appl. Pharmacol. 72*, 61−74.

40. Kim, D. H. (1999) Design of protease inhibitors on the basis of substrate stereospecificity, *Biopolymers 51*, 3−8.
41. Komiyama, M., and Bender, M. L. (1979) Do cleavages of amides by serine proteases occur through a stepwise pathway involving tetrahedral intermediates?, *Proc. Natl. Acad. Sci. U.S.A. 76*, 557−560.
42. Ekstrom, F., Akfur, C., Tunemalm, A. K., and Lundberg, S. (2006) Structural changes of phenylalanine 338 and histidine 447 revealed by the crystal structures of tabun-inhibited murine acetylcholinesterase, *Biochemistry 45*, 74−81.
43. Degenhardt, C. E. A. M., Van Den, Berg, G. R., de Jong, L. P., and Benschop, H. P. (1986) Enantiospecific Complexation Gas Chromotography of Nerve Agents. Isolation and Properties of the Enatiomers of Ethyl N,N-Dimethylphosphoramidocyanidate (tabun), *J. Am. Chem. Soc. 108*, 8290−8291.
44. Ordentlich, A., Barak, D., Sod-Moriah, G., Kaplan, D., Mizrahi, D., Segall, Y., Kronman, C., Karton, Y., Lazar, A., Marcus, D., Velan, B., and Shafferman, A. (2005) The role of AChE active site gorge in determining stereoselectivity of charged and noncharged VX enantiomers, *Chem. Biol. Interact. 157−158*, 191−198.
45. Langenberg, J. P., van Dijk, C., Sweeney, R. E., Maxwell, D. M., De Jong, L. P., and Benschop, H. P. (1997) Development of a physiologically based model for the toxicokinetics of C(+/−)P-(+/−)-soman in the atropinized guinea pig, *Arch. Toxicol. 71*, 320−331.
46. Binkowski, T. A., Naghibzadeh, S., and Liang, J. (2003) CASTp: Computed Atlas of Surface Topography of proteins, *Nucleic Acids Res. 31*, 3352−3355.
47. Sterri, S. H., and Fonnum, F. (1987) Carboxylesterases in guinea-pig plasma and liver. Tissue specific reactivation by diacetylmonoxime after soman inhibition in vitro, *Biochem. Pharmacol. 36*, 3937−3942.
48. Ekstrom, F., Pang, Y. P., Boman, M., Artursson, E., Akfur, C., and Borjegren, S. (2006) Crystal structures of acetylcholinesterase in complex with HI-6, Ortho-7 and obidoxime: structural basis for differences in the ability to reactivate tabun conjugates, *Biochem. Pharmacol. 72*, 597−607.
49. Lenz, D. E., Yeung, D., Smith, J. R., Sweeney, R. E., Lumley, L. A., and Cerasoli, D. M. (2006) Stoichiometric and catalytic scavengers as protection against nerve agent toxicity: A mini review, *Toxicology*. DOI: 10.1016.
50. Elhanany, E., Ordentlich, A., Dgany, O., Kaplan, D., Segall, Y., Barak, R., Velan, B., and Shafferman, A. (2001) Resolving pathways of interaction of covalent inhibitors with the active site of acetylcholinesterases: MALDI-TOF/MS analysis of various nerve agent phosphyl adducts, *Chem. Res. Toxicol. 14*, 912−918.
51. Gopal, S., Rastogi, V., Ashman, W., and Mulbry, W. (2000) Mutagenesis of organophosphorus hydrolase to enhance hydrolysis of the nerve agent VX, *Biochem. Biophys. Res. Commun. 279*, 516−519.
52. Lockridge, O., Blong, R. M., Masson, P., Froment, M. T., Millard, C. B., and Broomfield, C. A. (1997) A single amino acid substitution, Gly117His, confers phosphotriesterase (organophosphorus acid anhydride hydrolase) activity on human butyrylcholinesterase, *Biochemistry 36*, 786−795.
53. Cerasoli, D. M., Griffiths, E. M., Doctor, B. P., Saxena, A., Fedorko, J. M., Greig, N. H., Yu, Q. S., Huang, Y., Wilgus, H., Karatzas, C. N., Koplovitz, I., and Lenz, D. E. (2005) In vitro and in vivo characterization of recombinant human butyrylcholinesterase (Protexia) as a potential nerve agent bioscavenger, *Chem. Biol. Interact. 157-158*, 363−365.
54. Grimsley, J. K., Calamini, B., Wild, J. R., and Mesecar, A. D. (2005) Structural and mutational studies of organophosphorus hydrolase reveal a cryptic and functional allosteric-binding site, *Arch. Biochem. Biophys. 442*, 169−179.
55. Hill, C., Wen-Shan, L., Thoden, J., Holden, H., and Raushel, F. (2003) Enhanced Degredation of Chemical Warfare Agents through Molecular Engineering of the Phosphotriesterase Active Site, *J. Am. Chem. Soc. 125*, 8990−8991.

BI700246N